nature portfolio

https://doi.org/10.1038/s41586-021-03285-w

Supplementary information

Efficient perovskite solar cells via improved carrier management

In the format provided by the authors and unedited

Supplementary Information for:

Efficient perovskite solar cells via improved carrier management

Authors: Jason J. Yoo[1,8,9], Gabkyung Seo[2,7,9], Matthew R. Chua[3], Tae Gwan Park[4], Yongli Lu[1], Fabian Rotermund[4], Young-Ki Kim[5], Chan Su Moon[2], Nam Joong Jeon[2], Juan-Pablo Correa-Baena[6], Vladimir Bulović[3], Seong Sik Shin[2]†, Moungi G. Bawendi[1]† & Jangwon Seo[2]†

Affiliations:

[1]Department of Chemistry, Massachusetts Institute of Technology, Cambridge, MA, USA.

[2]Division of Advanced Materials, Korea Research Institute of Chemical Technology, Daejeon, Republic of Korea.

[3]Department of Electrical Engineering and Computer Science, Massachusetts Institute of Technology, Cambridge, MA, USA.

[4]Department of Physics, Korea Advanced Institute of Science and Technology, Daejeon, Republic of Korea.

[5]Center Research Facilities, Ulsan National Institute of Science and Technology (UNIST), Ulsan, Republic of Korea.

[6]School of Materials Science and Engineering, Georgia Institute of Technology, Atlanta, GA, USA.

[7]Department of Energy Science, Sungkyunkwan University, Suwon 16419, Republic of Korea.

[8]Present address: Division of Advanced Materials, Korea Research Institute of Chemical Technology, Daejeon, Republic of Korea.

[9]These authors contributed equally: Jason J. Yoo, Gabkyung Seo.

†e-mail: sss85@krict.re.kr; mgb@mit.edu; jwseo@krict.re.kr

Contents

Methods

Chemicals

DI water, urea, hydrochloric acid (HCl, 37 wt. % in water), thioglycolic acid (TGA, 98%), $SnCl_2 \cdot 2H_2O$ (>99.995%) , dimethylformamide (DMF), dimethyl sulfoxide (DMSO), diethyl ether, chlorobenzene, chloroform, isopropyl alcohol, lithium Bis(trifluoromethanesulfonyl)imide salt (Li-TFSI), and 4-tert-butylpyridine (tBP) were purchased from Sigma-Aldrich. 2,2',7,7'-Tetrakis(N,N -di-p -methoxyphenylamino)-9,9'-spirobifluorene (Spiro-OMeTAD, LT-S922) and Tris(2-(1H -pyrazol-1-yl)-4-tert-butylpyridine)-cobalt(III)Tris(bis(trifluoromethylsulfonyl)imide)) salt (Co(III) TFSI) were purchased from Lumtec. Methylammonium chloride (MACl) was purchased from Dyenamo. Formamidinium iodide (FAI), methylammonium bromide (MABr), and n-hexylammonium bromide were purchased from GreatCell Solar Materials. Lead iodide (PbI_2) and lead bromide ($PbBr_2$) were purchased from TCI America. Au pellets were purchased from Kurt J. Lesker.

Chemical Bath Deposition (CBD) of SnO_2 layer

The FTO substrate was cleaned by sonicating in Hellmanex solution, DI water, acetone, and IPA for 10 min each. The CBD solution was prepared by mixing 625 mg of urea, 625 μL of HCl, 12.5 μL of TGA, and 137.5 mg of $SnCl_2 \cdot 2H_2O$ per 50 mL of DI water. We noticed there is an obvious difference in solubility between low purity (>99.99%) and high purity (>99.995%) $SnCl_2 \cdot 2H_2O$. When dissolved in DI water, prior to adding HCl, the reaction solution with low purity source stays murky while the high purity source dissolves completely to yield a transparent solution. Thus, we strongly suggest using the high purity source (>99.995%). One edge of the FTO substrate was taped with a kapton tape to prevent deposition of SnO_2. The FTO substrates and the CBD solution were loaded onto a glass reaction vessel and reacted at 90 °C until the desired pH is reached. Specifically, we used a Hellendahl staining dish with the vessel volume of ~170 mL. Eight 1"x 1" FTO substrates were vertically placed inside the vessel and 50 mL of the

CBD solution were added. The reaction vessel was placed inside a water bath set to a target temperature. The pH of the reaction solution was monitored and the reaction was ended by removing the substrate at the target pH. It took 4 hrs to reach pH 1.5, 6hrs to reach pH 3, and 7 hrs to reach pH 6. The pH was measured after the solution cooled down to room temperature. After the reaction is complete, the SnO_2 deposited FTO substrate was removed from the reaction vessel and cleaned via sonication with DI water and IPA for 5min each.

Figure 2e shows the progress of the synthesis of SnO_2 via CBD. At the early stage of the reaction (Stage A-i), the SnO_2 layer does not fully cover the underlying FTO layer and poor film coverage with shallow valence band results in inefficient hole blocking capability, leading to detrimental interface recombination and poor device performance. When the reaction reaches Stage A-ii, high quality SnO_2 layer forms a compact and conformal film, providing sufficient coverage of the underlying TCO. The ideal morphology and chemical composition of SnO_2 ETL during Stage A-ii leads to an efficient extraction of the charge carrier from the perovskite layer without energy loss through non-radiative pathways, supported by high *FF* and V_{OC}, and ultimately the PCE. When the reaction continues past this "magic region", the SnO_2 layer contains unwanted site defects, as a form of oxygen vacancy, (Stage A-iii) and further the formation of secondary crystal phases (Stage B) inhibit efficient charge extraction and transport.[1,2] Our results show that careful engineering of the intrinsic and extrinsic properties of the ETL film, such as satisfying the coverage needed to prevent interfacial recombination, and suppressing the formation of detrimental defects, along with suppressing the formation of secondary crystal phases, is crucial for fabricating high performance PSCs.

Device fabrication

The FTO/SnO_2 substrate was annealed in an ambient environment (RH 15-30%) at 170 °C for 60 min, followed by spincoating10 mM KCl in DI water at 3000 rpm for 30

sec (2000 rpm ramp) and annealing at 100 °C for 10 min. All SnO_2 layers were equally treated with an aqueous solution of potassium chloride as such salts have been reported to reduce hysteresis, interface recombination, and improve luminescence.[3–5] Before perovskite deposition, the FTO/SnO_2 substrate was oxygen plasma treated and pumped inside a nitrogen glovebo x.

We used a FA-based perovskite composition with excess PbI_2 stoichiometry (9 mol%), due to its positive effect in enhancing device performance[6,7], and with MACl as an additive, due to its role in stabilizing the intermediate phase and enhancing perovskite orientation.[8,9] The perovskite solution was prepared by mixing 1.53 M PbI_2, 1.4 M FAI, 0.5 M MACl, and 0.0122 M (0.8 mol%)-0.153 M (10 mol%) $MAPbBr_3$ in DMF:DMSO=8:1. The perovskite solution deposited via spin coating at 1000 rpm for 10 sec, and 5000 rpm for 30 sec (both 2000 rpm ramp). 10 seconds into the 5000 rpm setting, 600 μL of diethyl ether solution was deposited onto the substrate. Afterwards, the FTO/SnO_2/perovskite substrate was annealed at 100 °C for 60 min. For the 2D perovskite passivation, 10 mM of alkylammonium bromide was deposited at 3000 rpm for 30 sec and annealed at 100 °C for 5 min.

The hole transporting layer (HTL) was deposited by preparing the HTL solution consisting of 50 mg of Spiro-OMeTAD, 19.5 μL of tBP, 5 μL of Co(III) TFSI solution (0.25 M in acetonitrile), 11.5 μL of Li-TFSI solution (1.8 M in acetonitrile), and 547 μL of chlorobenzene. 70 μL of the HTL solution was loaded onto the perovskite substrate and spin coated at 4000 rpm for 20 sec with the ramp of 2000 rpm/sec. The HTL solution preparation and deposition were performed inside a nitrogen glovebox. The Au electrode (100 nm) was deposited by thermal evaporation.

Device Characterization

Current density-voltage (*J-V*) curves were recorded using a solar simulator (Newport, Oriel Class AAA, 91195A) and a source meter (Keithley 2420). The illumination was set to AM 1.5G and calibrated to 100 mW/cm^2 using a calibrated silicon reference cell. The step voltage was 10 mV and the delay time was 50 ms. The active area was controlled by using a dark mask with a defined aperture.

Long-term stability (Supplementary Figure 23) was performed by tracking the maximum power point (MPP) under continuous illumination (Newport, Oriel Class ABA, 94062A, AM 1.5G, 100 mW/cm^2), in a nitrogen environment. Our long-term stability follows ISOS-L-1I testing protocol (Light source: solar simulator, temperature: ambient, rel. humidity: ambient, environment/set-up: lightly only, characterization light source: solar simulator, Load: MPP). The stability test was performed without active cooling and the device temperature is measured to be ~45 °C.[10]

Scanning Electron Microscope (SEM) and X-ray Diffraction (XRD)

The SEM images were recorded using a Zeiss Merlin High-resolution SEM and the XRD patterns were collected using a Rigaku SmartLab and a Bruker D8 Discovery Diffractometer with a General Area Detector Diffraction System.

Cyclic Voltammetry (CV)

CV measurement was performed using potentiostat (AUTOLAB PGSTAT 302N, Metrohm Autolab) with 0.1V/s of scan rate in a three-electrode configuration using a saturated calomel electrode (SCE) as reference electrode, Pt counter electrode, and the synthesized films as working electrode under dark condition. 0.5 M KCl aqueous solution added 0.5 mM potassium ferricyanide and 0.5 mM potassium hexacyano-ferrate was used as the electrolyte.

UVVis and photoluminescence measurement

UVVis was recorded using Cary UV-Vis-NIR spectrophotometer. The PL was recorded using a SpectraPro monochromator and PIXIS CCD from Princeton Instruments with 532 nm exciation using a laser diode from Thorlabs.

Electroluminescence (EL) Characterization

The devices were encapsulated and the EL was measured under ambient conditions in the dark. The device was voltage driven, and the current was measured simultaneously by a Keithley 2636A sourcemeter. The photocurrent was collected using a calibrated Newport 818-UV/DB Silicon photodetector coupled to a Newport 1835-C Multifunction Optical meter. EL spectra are collected using an Ocean Optics USB 2000 spectrometer using a multimode fiber positioned over the center of the active area. The I-V-Photocurrent sweep was run by a custom Labview code with the sweep rate of 5 mV/s.

Transient photovoltage (TPV) and photocurrent (TPC)

The photovoltaic devices were electrically connected to a digital oscilloscope (500 MHz, DSO-X 3054A, Agilent) with BNC cables. To obtain charge decay time of open-circuit and charge extraction time of short-circuit, the input impedance of oscilloscope was set to be 1 MΩ and 50 Ω for open circuit condition and short circuit condition, respectively. The TPV and TPC were measured under 0.346 Sun illumination by light source of Xe lamp (Zolix, 150W), and were taken using a nanosecond laser of the 532 nm excitation (EKSPLA, NT342A-10) as a small perturbation.

Time Resolved Photoluminescence

Time resolved photoluminescence lifetimes were collected using a 532 nm picosecond pulsed diode laser (Picoquant; LDH-P-FA-530-B) adjusted the repetition rate using a pulse generator (Stanford Research; DG535). The excitation power was adjusted using neutral density filters and focused to a spot size of ~100 μm in diameter. The emission from the film was collected and collimated using an off-axis parabolic mirror (Thorlabs; MPD269V) and measured with a silicon single-photon avalanche diode (SPAD) detector (Micro Photon Devices; $PD-100-C0C). Scattered laser excitation was suppressed using a 532 nm notch filter (Chroma; ZET532NF) and a 550 nm longpass filter (Thorlabs; FELH0550). The 532 nm laser harmonic was suppressed using a 900 nm shortpass filter (Thorlabs; FESH0900). Photon arrival times were recorded using a time-correlated single photon counting card (Picoquant; PicoHarp 300) and all analysis was performed in Matlab. The carrier density was 1.125×10^{15} cm^{-3}.

Optical Pump - THz Probe (OPTP) Spectroscopy.

The perovskite thin films for OPTP was prepared by using 0.5 M concentration with same spin coating parameters. The time-resolved optical pump and THz probe spectroscopy was performed by utilizing 100-fs laser pulses generated from a 1-kHz Ti:sapphire regenerative amplifier (Spitfire Ace Pro, Spectra Physics) operating at 800 nm. Optical pump pulses at 400 nm were achieved by second harmonic generation in a beta barium borate (BBO) crystal, whereas THz pulses serving as the probe beam were generated by optical rectification in a 2-mm-thick ZnTe crystal and detected by electro-optic sampling method. The pump-induced THz transmission changes were then measured by using a lock-in-Amplifier (SR830, Stanford Research Systems) depending on the time delay between the pump and probe beams controlled by a motorized stage, while the 400-nm pump pulses were modulated at 190 Hz by the optical chopper. All the measurements were performed under 2% humidity by purging the entire THz beam path with dry air.

Supplementary Figures

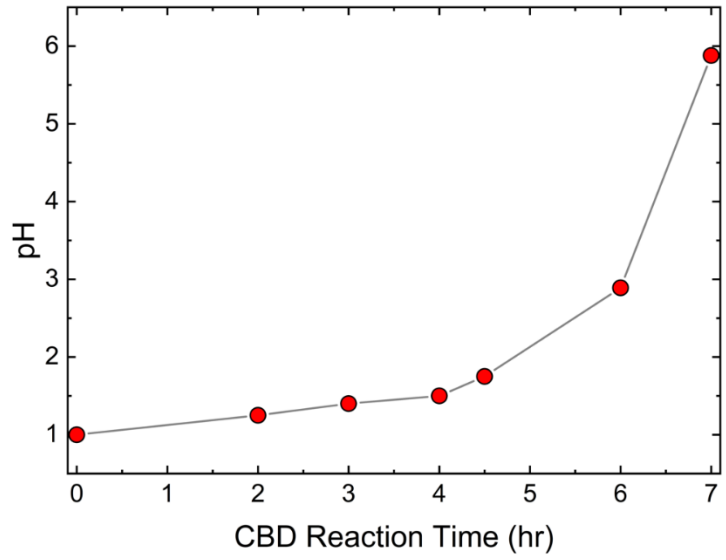

Supplementary Figure 1.

Plot of pH versus reaction time.

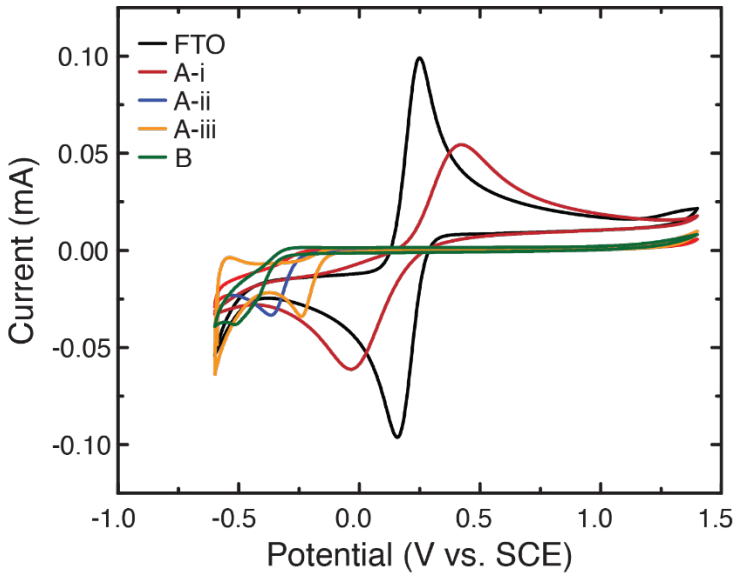

Supplementary Figure 2.

Cyclic voltammograms of bare FTO and SnO_2 ETL synthesized up to various reaction stages (A-i through B). The scan rate was 0.1 V/s and the electrolyte solution was 0.5 mM $K_4Fe(CN)_6$ + 0.5 mM $K_3Fe(CN)_6$ in 0.5M aqueous KCl. A saturated calomel electrode (SCE) is used as the reference electrode.

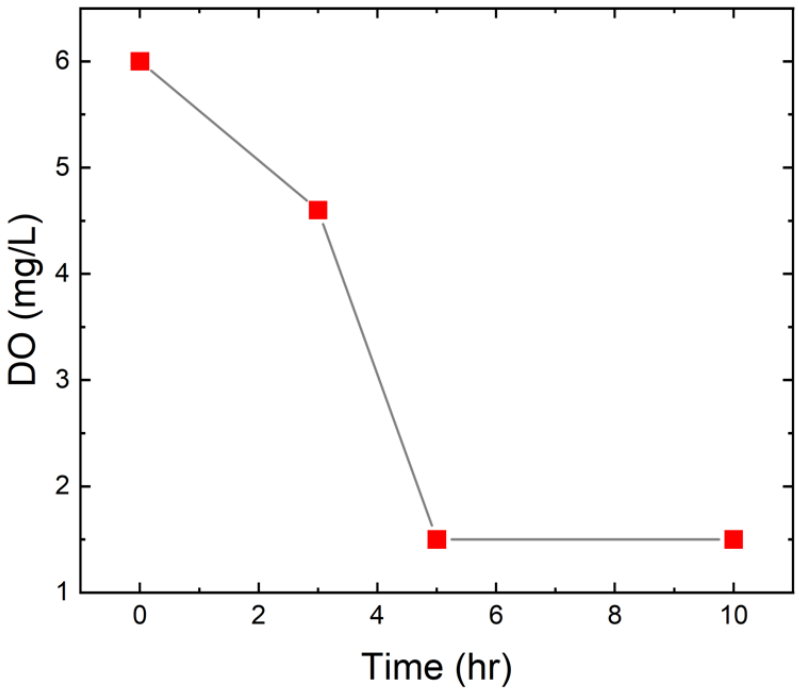

Supplementary Figure 3.

Tracking of dissolved oxygen (DO) at 90 °C for 10hrs. DO was measured after the solution is been cooled to room temperature.

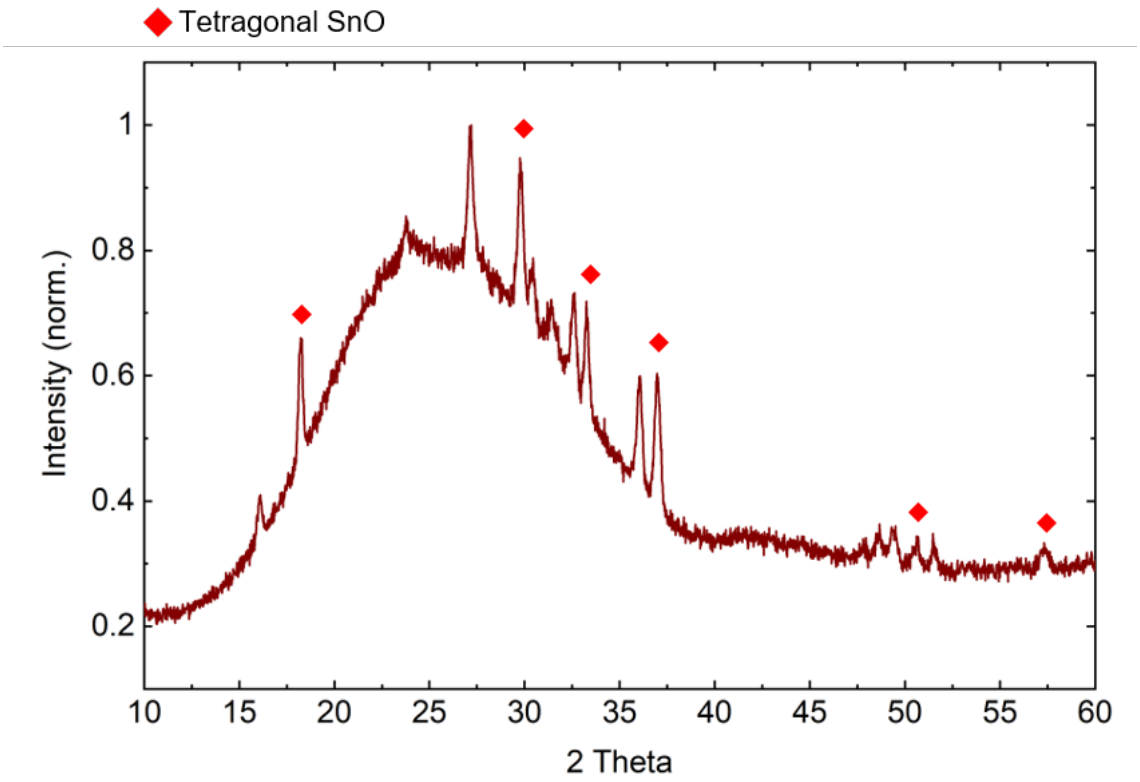

Supplementary Figure 4.

XRD pattern of the red precipitates shown in Figure 1h. The precipitate was separated from the reaction solution, spin-coated onto a glass substrate, and annealed in ambient air at 170 °C for 1hr.

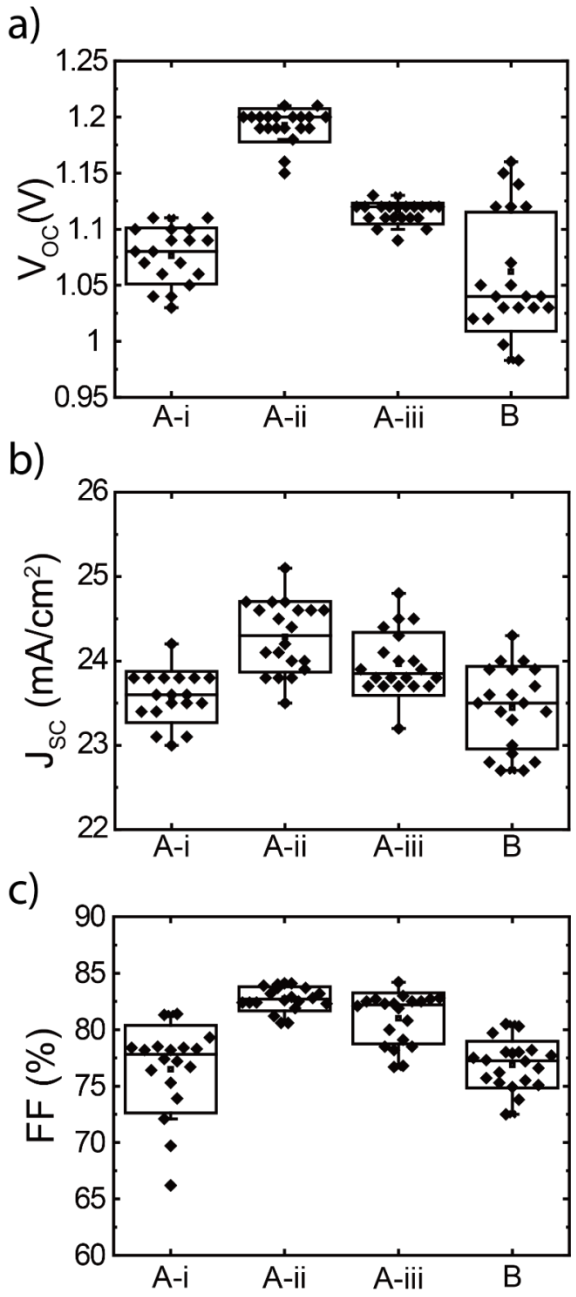

Supplementary Figure 5.

Device statistics represented in box-and-whisker plots (center line: average, box limit: standard deviation, whiskers: outliers) for the open-circuit voltage (V_{OC}) (a), the short-circuit current density (J_{SC}) (b), and the fill factor (FF) (c) for the devices with various SnO_2 ETL synthesized up to various stages (Stage A-i through B).

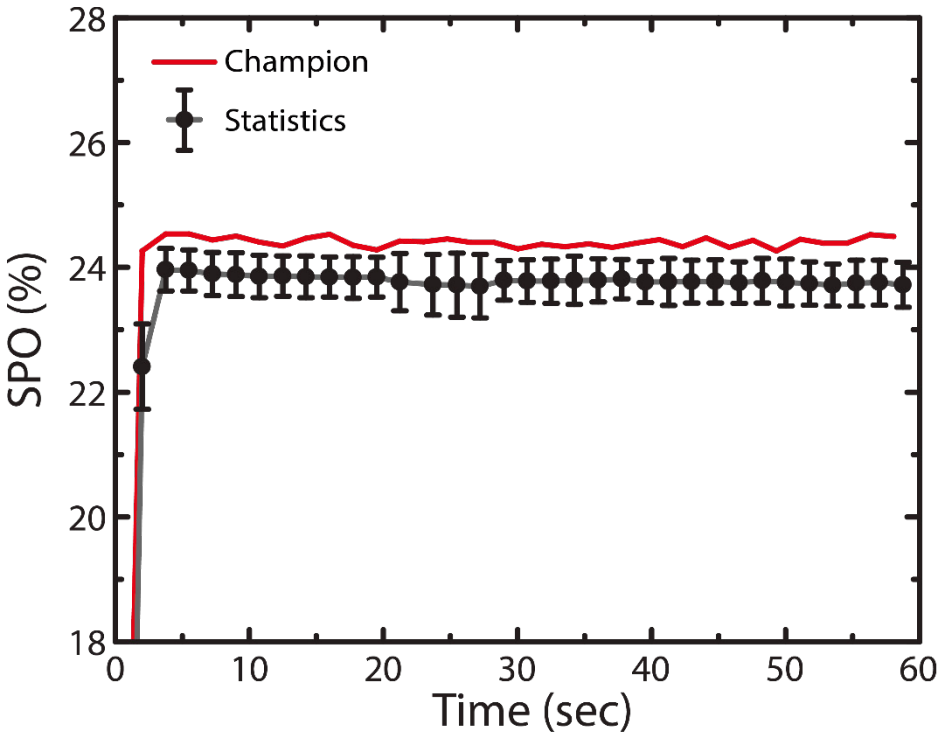

Supplementary Figure 6.

Stabilized power output (SPO) for 16 PSCs with a SnO_2 ETL fabricated until Stage A-ii. The black trace is the average statistics (error bars: SD) and the red trace is the champion device with SPO reaching up to 24.5%.

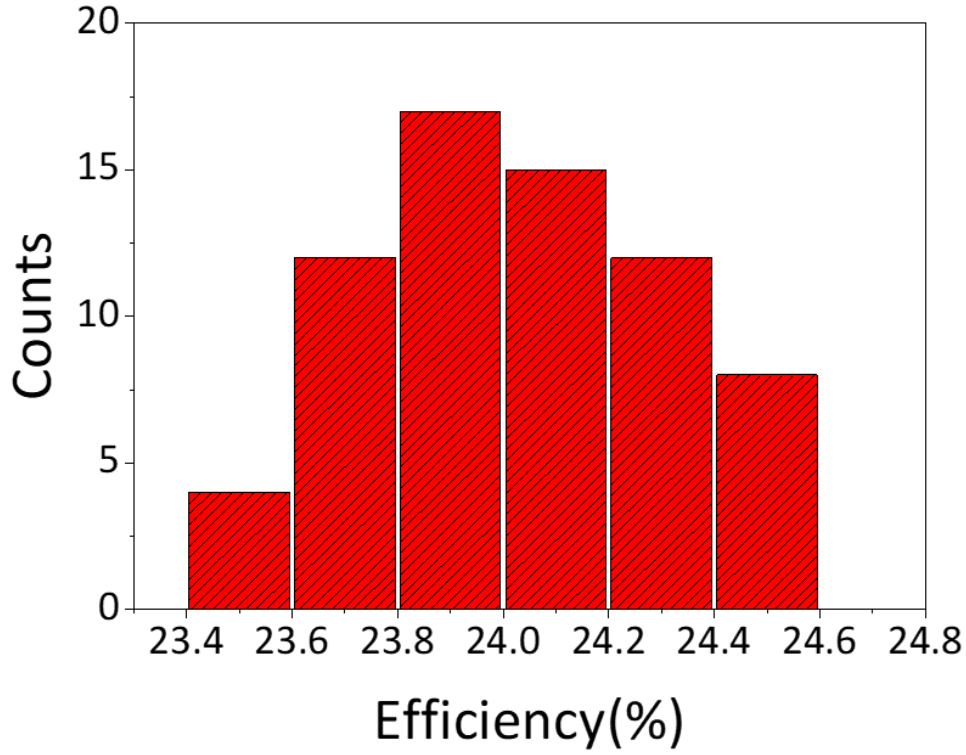

Supplementary Figure 7.

Histogram of device efficiency for 68 devices with Stage A-ii SnO_2 ETL.

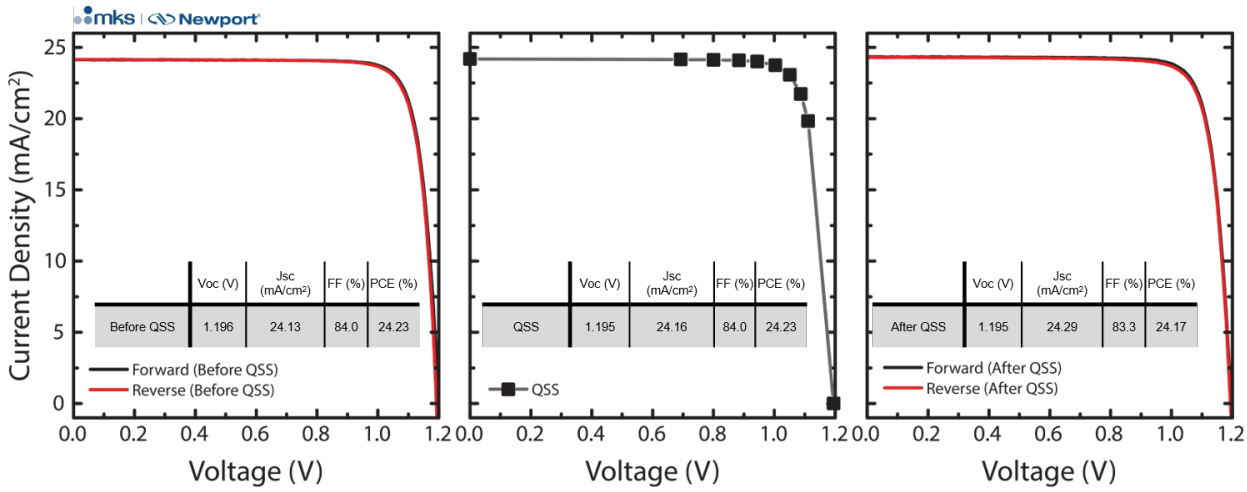

Supplementary Figure 8.

J-V curves before and after stabilization, and QSS J-V curve of the best-performing device (Stage A-ii). The device exhibits a PCE of 24.2% from the QSS measurement. The inset tables show the average device performance from the reverse and the forward *J-V* sweep.

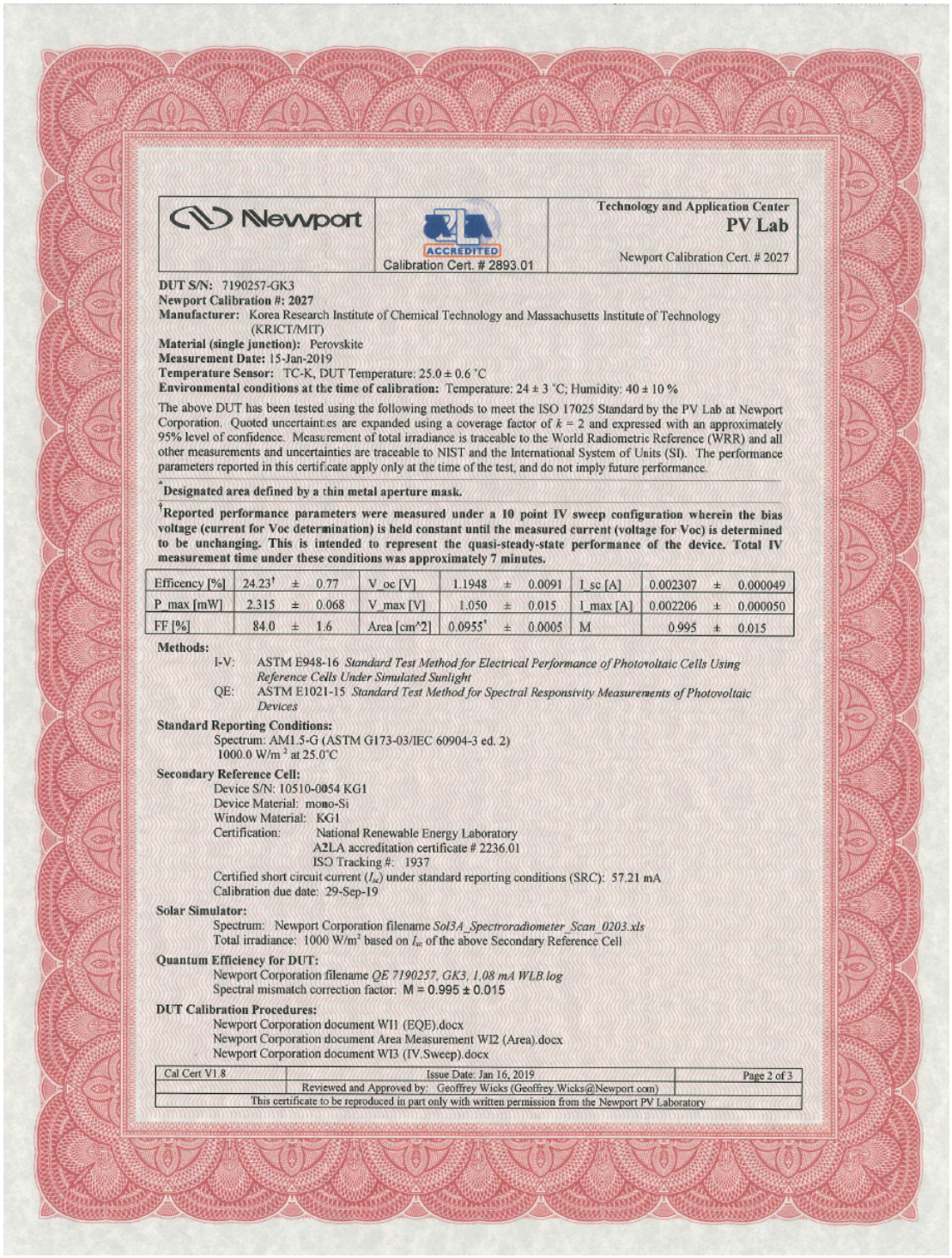

Newport

ACCREDITED
Calibration Cert. # 2893.01

Technology and Application Center
PV Lab
Newport Calibration Cert. # 2027

DUT S/N: 7190257-GK3
Newport Calibration #: 2027
Manufacturer: Korea Research Institute of Chemical Technology and Massachusetts Institute of Technology (KRICT/MIT)
Material (single junction): Perovskite
Measurement Date: 15-Jan-2019
Temperature Sensor: TC-K, DUT Temperature: 25.0 ± 0.6 °C
Environmental conditions at the time of calibration: Temperature: 24 ± 3 °C; Humidity: 40 ± 10 %

The above DUT has been tested using the following methods to meet the ISO 17025 Standard by the PV Lab at Newport Corporation. Quoted uncertainties are expanded using a coverage factor of $k = 2$ and expressed with an approximately 95% level of confidence. Measurement of total irradiance is traceable to the World Radiometric Reference (WRR) and all other measurements and uncertainties are traceable to NIST and the International System of Units (SI). The performance parameters reported in this certificate apply only at the time of the test, and do not imply future performance.

[*] Designated area defined by a thin metal aperture mask.

[†] Reported performance parameters were measured under a 10 point IV sweep configuration wherein the bias voltage (current for Voc determination) is held constant until the measured current (voltage for Voc) is determined to be unchanging. This is intended to represent the quasi-steady-state performance of the device. Total IV measurement time under these conditions was approximately 7 minutes.

Efficency [%]	24.23[†]	±	0.77	V_oc [V]	1.1948	±	0.0091	I_sc [A]	0.002307	±	0.000049
P_max [mW]	2.315	±	0.068	V_max [V]	1.050	±	0.015	I_max [A]	0.002206	±	0.000050
FF [%]	84.0	±	1.6	Area [cm^2]	0.0955[*]	±	0.0005	M	0.995	±	0.015

Methods:
I-V: ASTM E948-16 *Standard Test Method for Electrical Performance of Photovoltaic Cells Using Reference Cells Under Simulated Sunlight*
QE: ASTM E1021-15 *Standard Test Method for Spectral Responsivity Measurements of Photovoltaic Devices*

Standard Reporting Conditions:
Spectrum: AM1.5-G (ASTM G173-03/IEC 60904-3 ed. 2)
1000.0 W/m^2 at 25.0°C

Secondary Reference Cell:
Device S/N: 10510-0054 KG1
Device Material: mono-Si
Window Material: KG1
Certification: National Renewable Energy Laboratory
A2LA accreditation certificate # 2236.01
ISO Tracking #: 1937
Certified short circuit current (I_{sc}) under standard reporting conditions (SRC): 57.21 mA
Calibration due date: 29-Sep-19

Solar Simulator:
Spectrum: Newport Corporation filename *Sol3A_Spectroradiometer_Scan_0203.xls*
Total irradiance: 1000 W/m^2 based on I_{sc} of the above Secondary Reference Cell

Quantum Efficiency for DUT:
Newport Corporation filename *QE 7190257, GK3, 1.08 mA WLB.log*
Spectral mismatch correction factor: M = 0.995 ± 0.015

DUT Calibration Procedures:
Newport Corporation document WI1 (EQE).docx
Newport Corporation document Area Measurement WI2 (Area).docx
Newport Corporation document WI3 (IV.Sweep).docx

Supplementary Figure 9.

Certification of PSC efficiency exhibiting QSS PCE of 24.23% obtained from a device with Stage A-ii SnO_2 ETL.

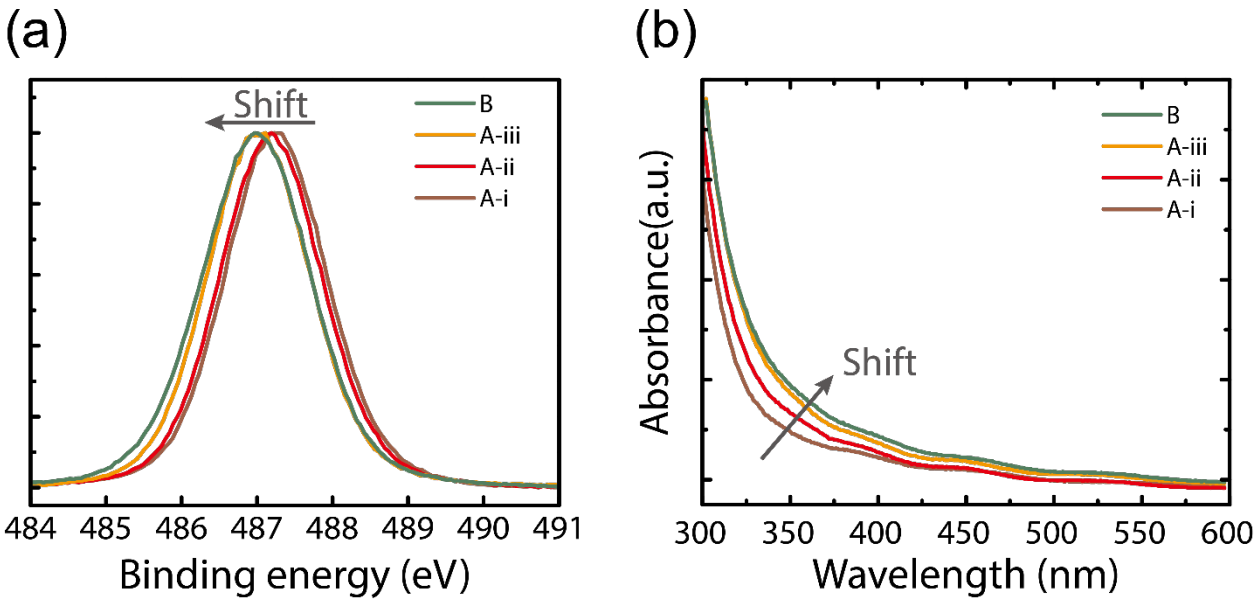

Supplementary Figure 10.

(a) XPS Sn $3d_{5/2}$ spectra, and (b) UV-Vis absorption spectra of SnO_2 films synthesized up to different reaction stages.

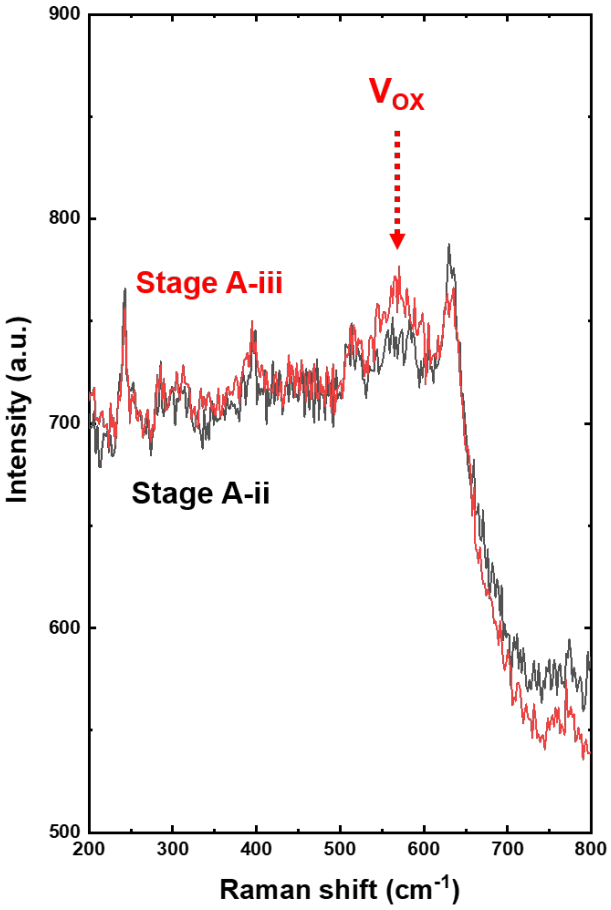

Supplementary Figure 11

Raman spectra for two different SnO_2 samples: Stage A-ii (black) and Stage A-iii (red). Increase in the peak that corresponds to oxygen vacancy (V_{OX}) at ~570 cm^{-1} is observed for the Stage A-iii sample.[11]

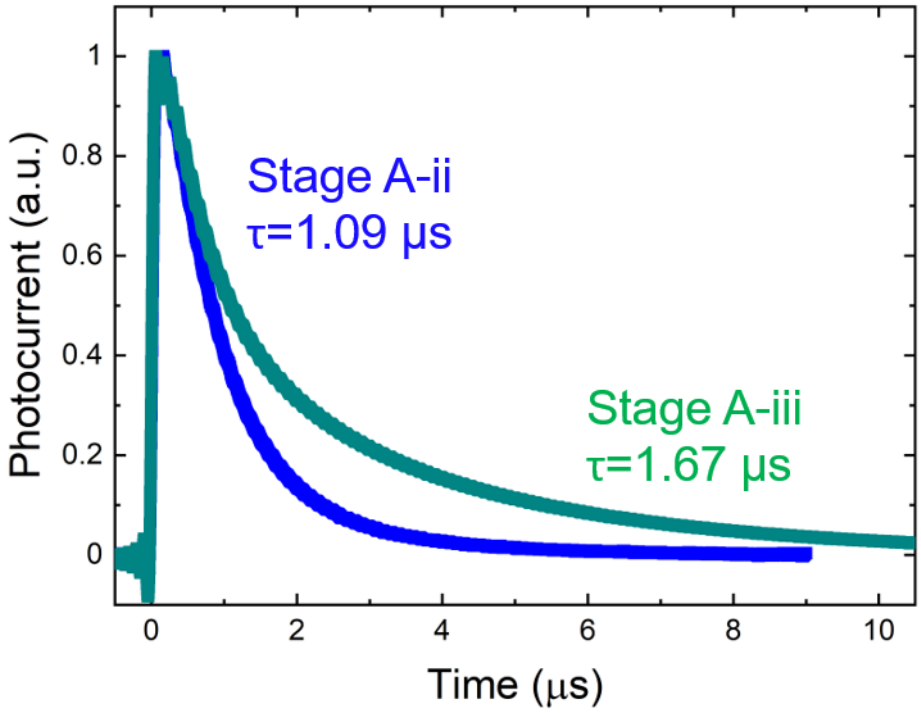

Supplementary Figure 12

Transient photocurrent (TPC) traces for perovskite solar cells with different SnO_2 ETL. The decay time is determined as the time it takes to reach 1/e intensity.

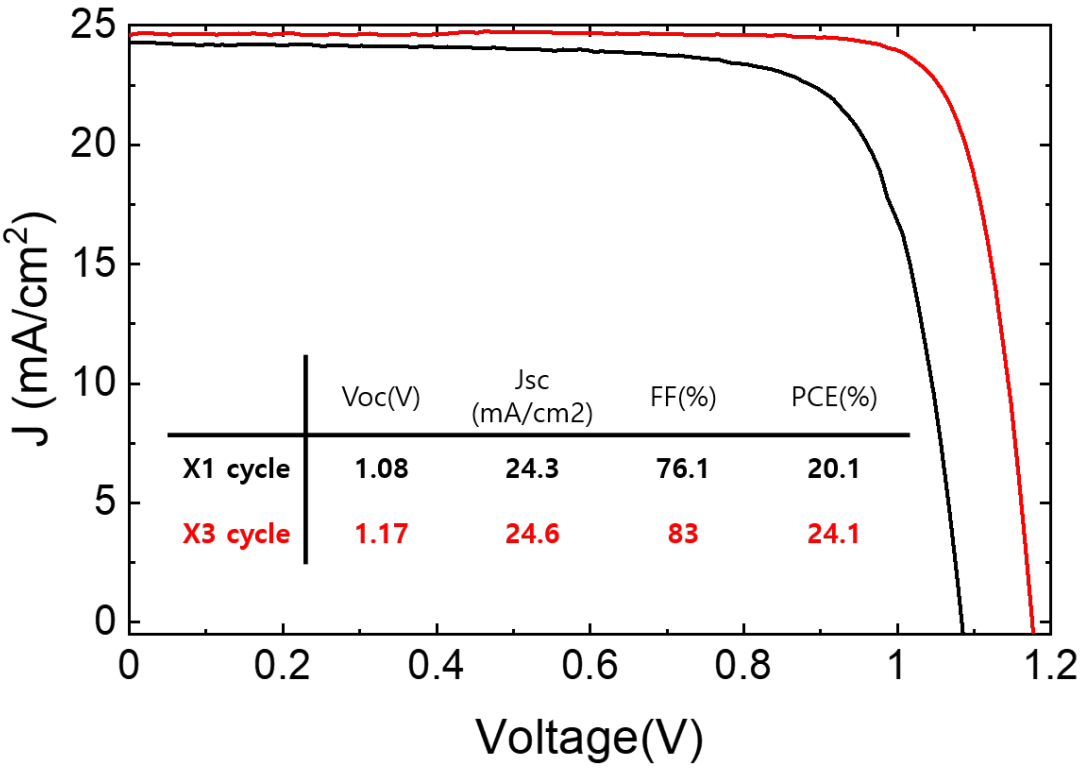

Supplementary Figure 13

J-V curves for PSC fabricated with different CBD reaction cycle. x1 cycle indicate single CBD reaction with short reaction times (2hr), while x3 cycle indicate three successive CBD reaction each with freshly prepared solution. Significant increase in the FF is due to improved coverage and high V_{OC} is due to SnO_2 layer with low defects (oxygen vacancies). Based on this experimental result, which was designed through our synthetic understanding of SnO_2 CBD, we believe highly efficient perovskite solar cells can also be achieve by adjusting relevant parameters, such as the reaction time and the number of reaction cycles.

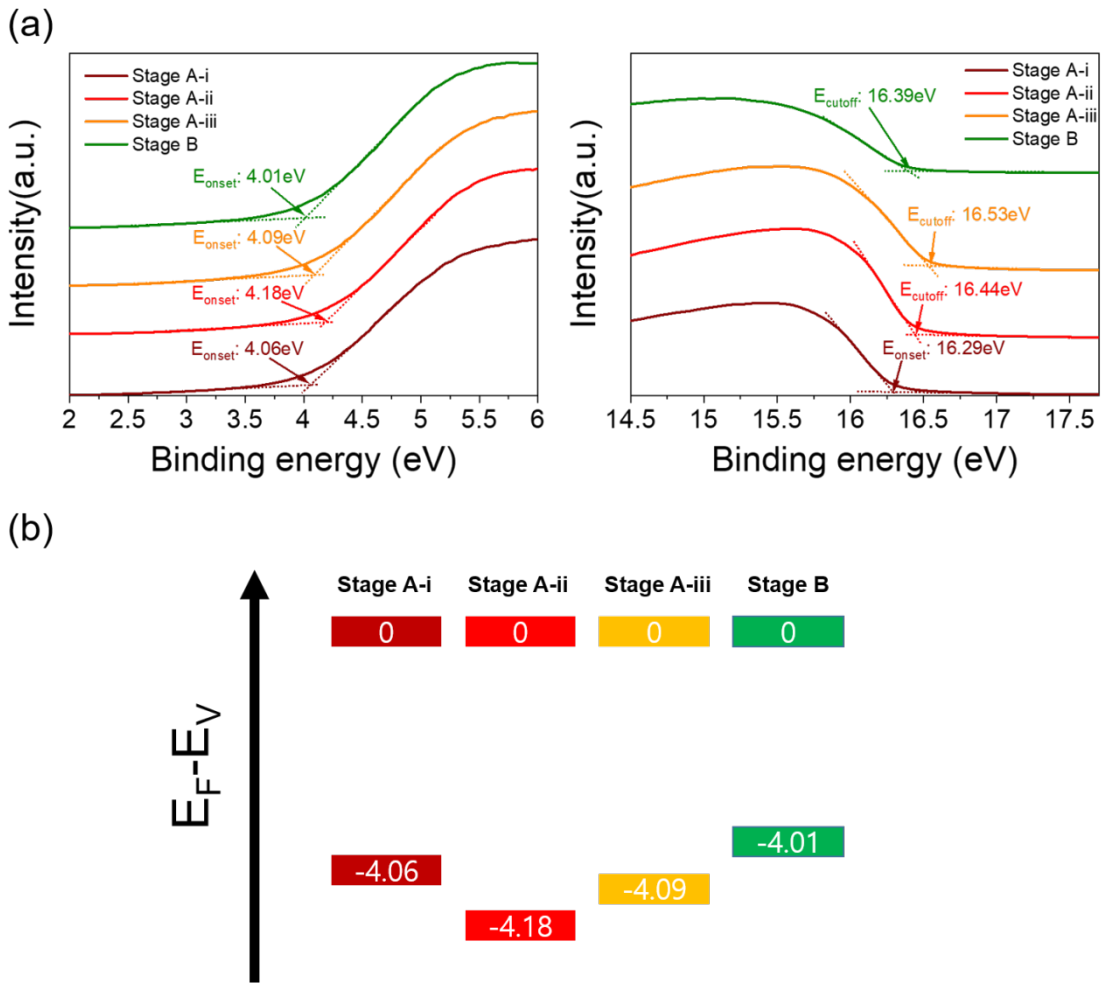

Supplementary Figure 14.

(a) UPS spectra of four SnO_2 samples (Stage A-i through B) prepared using CBD. The energy onset (E_{onset}) and cutoff (E_{cutoff}) are determined as the intersection between the extrapolated baseline and the slope. (b) Summary of the relative energy levels (E_F-E_V) determined from UPS results, where E_F is the work function and E_V is the valence band maximum.

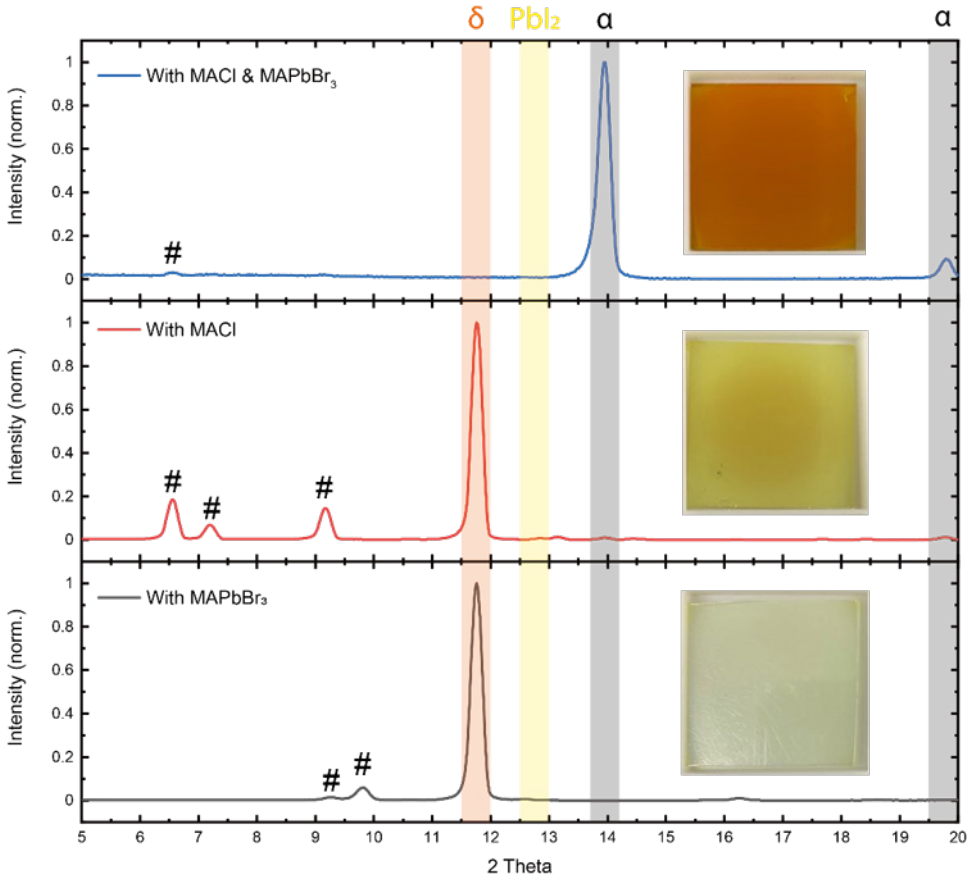

Supplementary Figure 15.

XRD pattern and photograph (inset) for three different samples immediately after anti-solvent treatment without any thermal annealing. The samples are: $FAPbI_3$ with only $MAPbBr_3$ (black trace), $FAPbI_3$ with only MACl (red trace), and $FAPbI_3$ with both MACl and $MAPbBr_3$ added (blue trace). The concentration for $MAPbBr_3$ is 0.8 mol% and 0.5 M for MACl. Only when a trace amount of MAPbBr3 is added along with MACl can we achieve an α-$FAPbI_3$ stabilized intermediate phase. Peaks labeled as # correspond to intermediate phases.

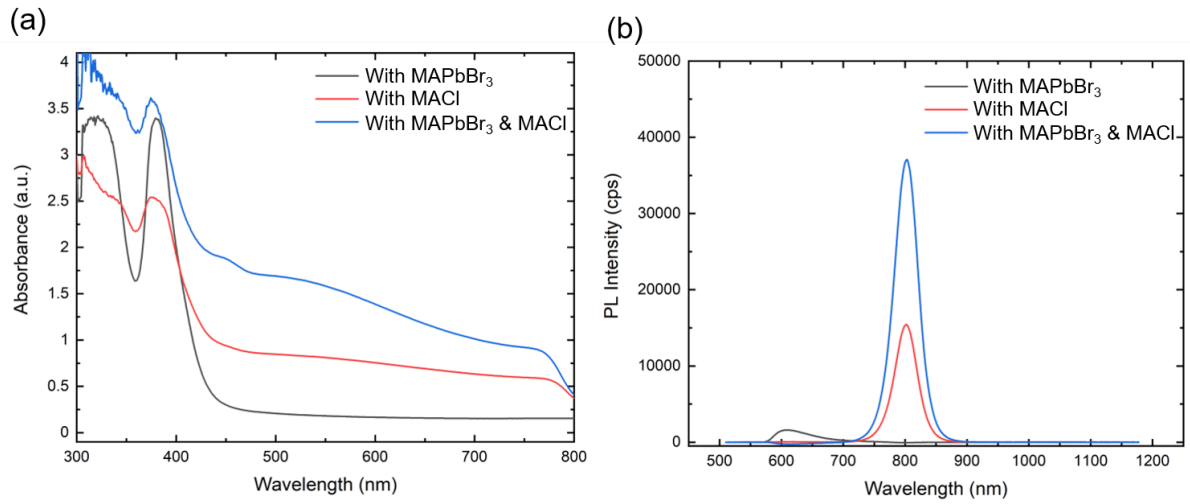

Supplementary Figure 16

UVVis absorption spectra (a) and PL spectra (b) for $FAPbI_3$ perovskite with different additives.

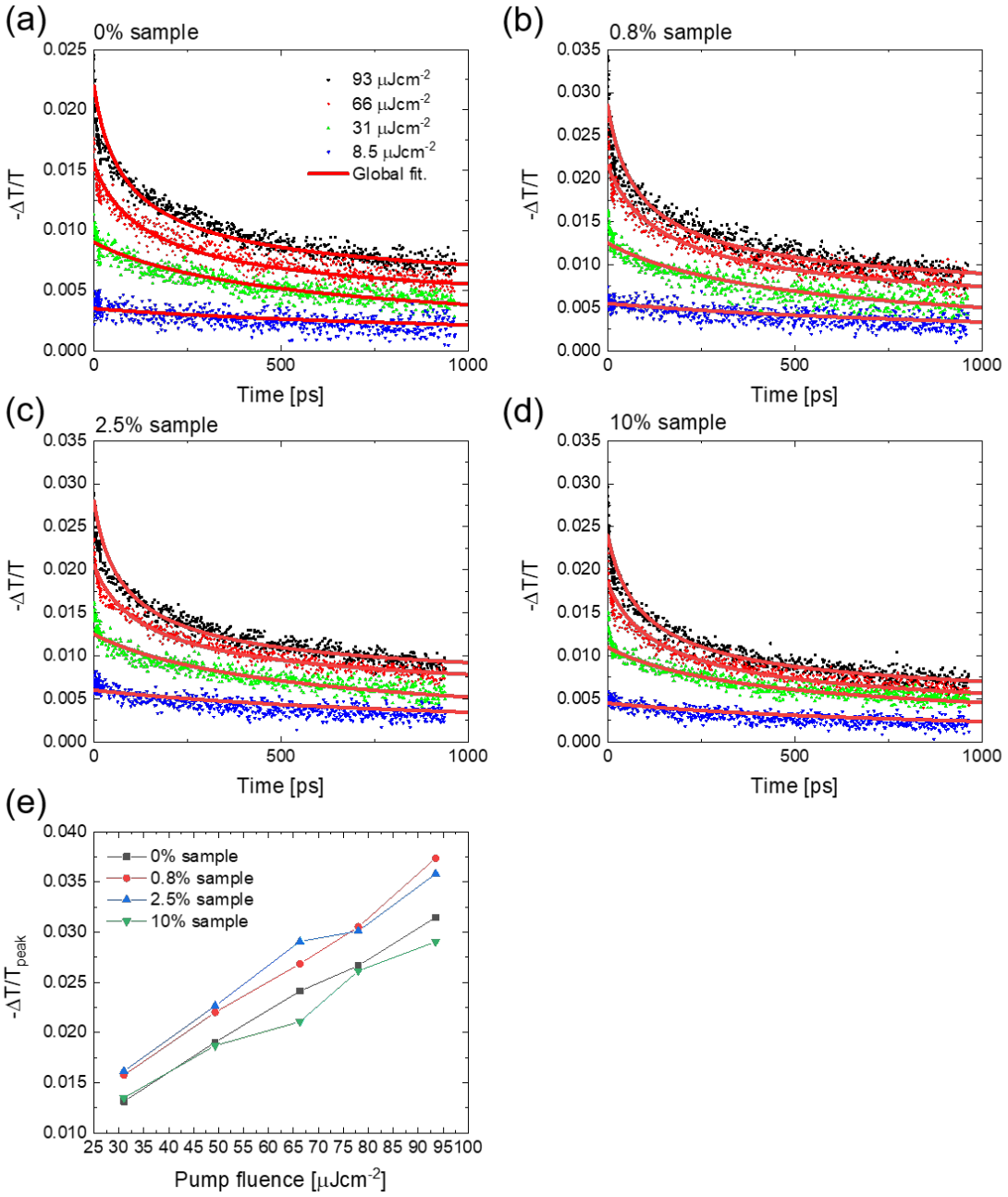

Supplementary Figure 17.

Optical-pump terahertz-probe (OPTP) traces for 0 mol% (a), 0.8 mol% (b), 2.5 mol% (c), and 10 mol% (d) of $MAPbBr_3$ added. (e) Plot of $-\Delta T/T_{peak}$ versus pump fluence for all perovskite composition.

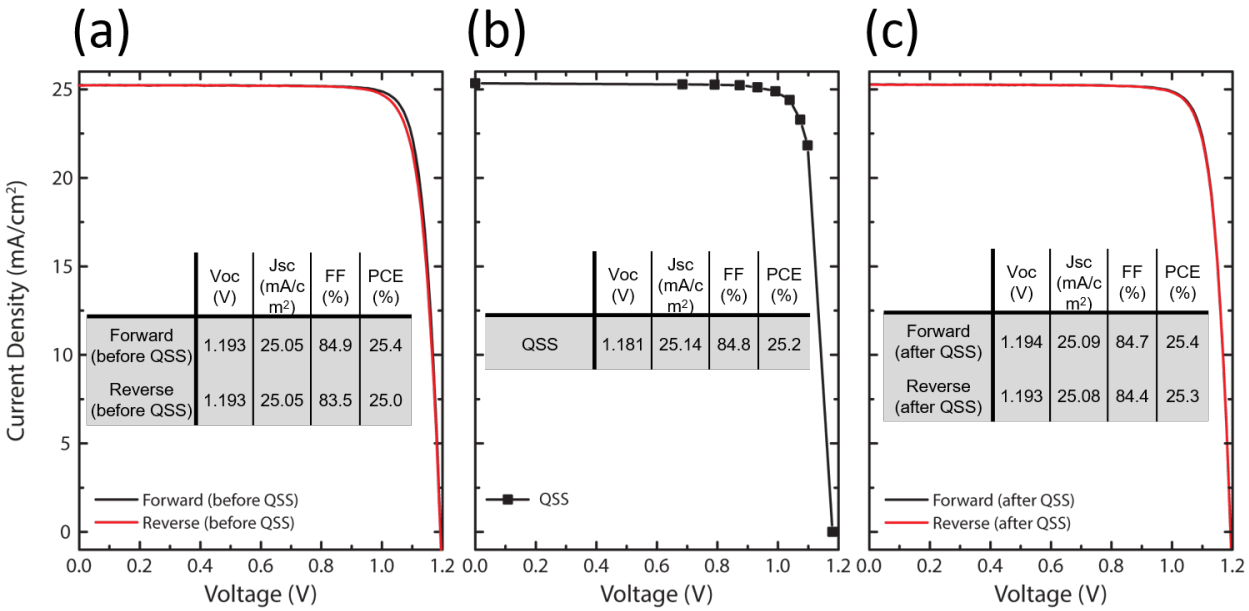

Supplementary Figure 18.

Sweep *J-V* curves of the champion PSC before QSS (a), QSS *J-V* curve (b), and sweep *J-V* curve after QSS measurement (c).

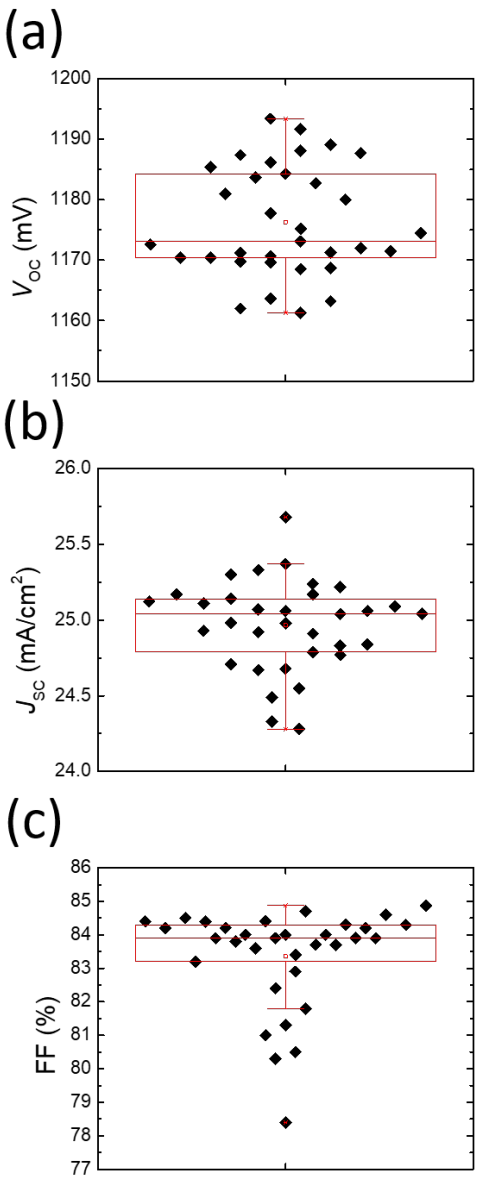

Supplementary Figure 19.

Device statistics represented in box-and-whisker plots (center line: average, box limit: standard deviation, whiskers: outliers) for the open-circuit voltage (V_{OC}) (a), the short-circuit current density (J_{SC}) (b), and the fill factor (FF) (c) for the best performing devices with Stage A-ii SnO_2 ETL and 0.8 mol% $MAPbBr_3$.

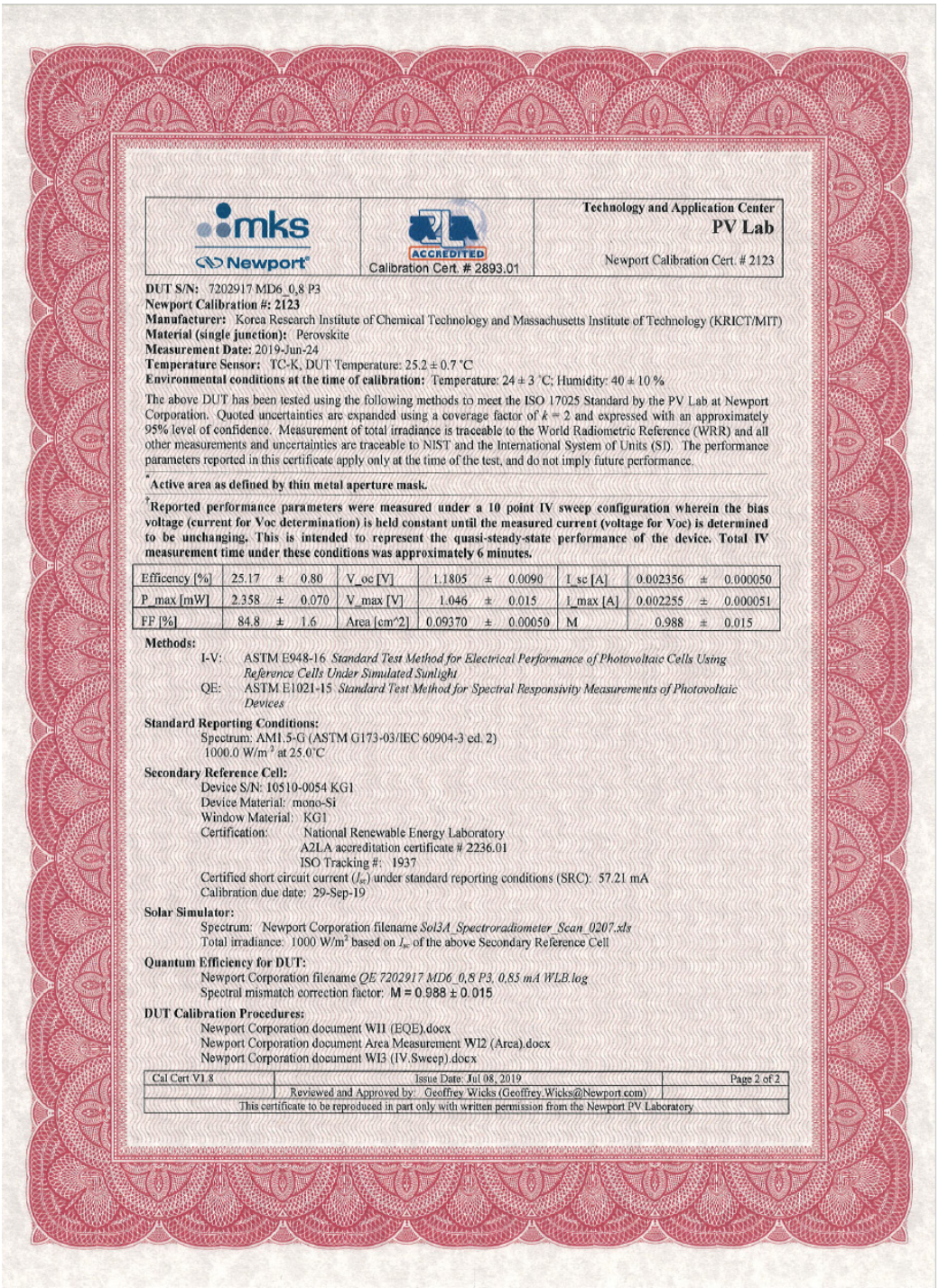

mks Newport

ACCREDITED Calibration Cert. # 2893.01

Technology and Application Center
PV Lab
Newport Calibration Cert. # 2123

DUT S/N: 7202917 MD6_0,8 P3
Newport Calibration #: 2123
Manufacturer: Korea Research Institute of Chemical Technology and Massachusetts Institute of Technology (KRICT/MIT)
Material (single junction): Perovskite
Measurement Date: 2019-Jun-24
Temperature Sensor: TC-K, DUT Temperature: 25.2 ± 0.7 °C
Environmental conditions at the time of calibration: Temperature: 24 ± 3 °C; Humidity: 40 ± 10 %

The above DUT has been tested using the following methods to meet the ISO 17025 Standard by the PV Lab at Newport Corporation. Quoted uncertainties are expanded using a coverage factor of $k = 2$ and expressed with an approximately 95% level of confidence. Measurement of total irradiance is traceable to the World Radiometric Reference (WRR) and all other measurements and uncertainties are traceable to NIST and the International System of Units (SI). The performance parameters reported in this certificate apply only at the time of the test, and do not imply future performance.

*Active area as defined by thin metal aperture mask.

†Reported performance parameters were measured under a 10 point IV sweep configuration wherein the bias voltage (current for Voc determination) is held constant until the measured current (voltage for Voc) is determined to be unchanging. This is intended to represent the quasi-steady-state performance of the device. Total IV measurement time under these conditions was approximately 6 minutes.

Efficency [%]	25.17	±	0.80	V_oc [V]	1.1805	±	0.0090	I_sc [A]	0.002356	±	0.000050
P_max [mW]	2.358	±	0.070	V_max [V]	1.046	±	0.015	I_max [A]	0.002255	±	0.000051
FF [%]	84.8	±	1.6	Area [cm^2]	0.09370	±	0.00050	M	0.988	±	0.015

Methods:
I-V: ASTM E948-16 *Standard Test Method for Electrical Performance of Photovoltaic Cells Using Reference Cells Under Simulated Sunlight*
QE: ASTM E1021-15 *Standard Test Method for Spectral Responsivity Measurements of Photovoltaic Devices*

Standard Reporting Conditions:
Spectrum: AM1.5-G (ASTM G173-03/IEC 60904-3 ed. 2)
1000.0 W/m² at 25.0°C

Secondary Reference Cell:
Device S/N: 10510-0054 KG1
Device Material: mono-Si
Window Material: KG1
Certification: National Renewable Energy Laboratory
A2LA accreditation certificate # 2236.01
ISO Tracking #: 1937
Certified short circuit current (I_{sc}) under standard reporting conditions (SRC): 57.21 mA
Calibration due date: 29-Sep-19

Solar Simulator:
Spectrum: Newport Corporation filename *Sol3A_Spectroradiometer_Scan_0207.xls*
Total irradiance: 1000 W/m² based on I_{sc} of the above Secondary Reference Cell

Quantum Efficiency for DUT:
Newport Corporation filename *QE 7202917 MD6_0,8 P3, 0,85 mA WLB.log*
Spectral mismatch correction factor: M = 0.988 ± 0.015

DUT Calibration Procedures:
Newport Corporation document WI1 (EQE).docx
Newport Corporation document Area Measurement WI2 (Area).docx
Newport Corporation document WI3 (IV.Sweep).docx

Cal Cert V1.8	Issue Date: Jul 08, 2019	Page 2 of 2
	Reviewed and Approved by: Geoffrey Wicks (Geoffrey.Wicks@Newport.com)	
This certificate to be reproduced in part only with written permission from the Newport PV Laboratory		

Supplementary Figure 20.

Certification of a PSC efficiency exhibiting stabilized efficiency of 25.2% obtained from a device with Stage A-ii SnO_2 ETL and 0.8 mol% $MAPbBr_3$.

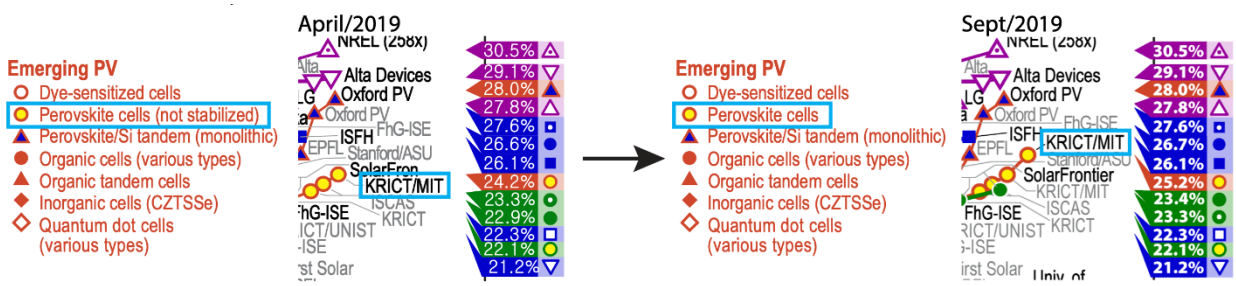

Supplementary Figure 21.

Solar cell efficiency chart published by NREL. The PSCs are no longer categorized as "not stabilized" as of September 2019 (Courtesy of the National Renewable Energy Laboratory, Golden, CO.).

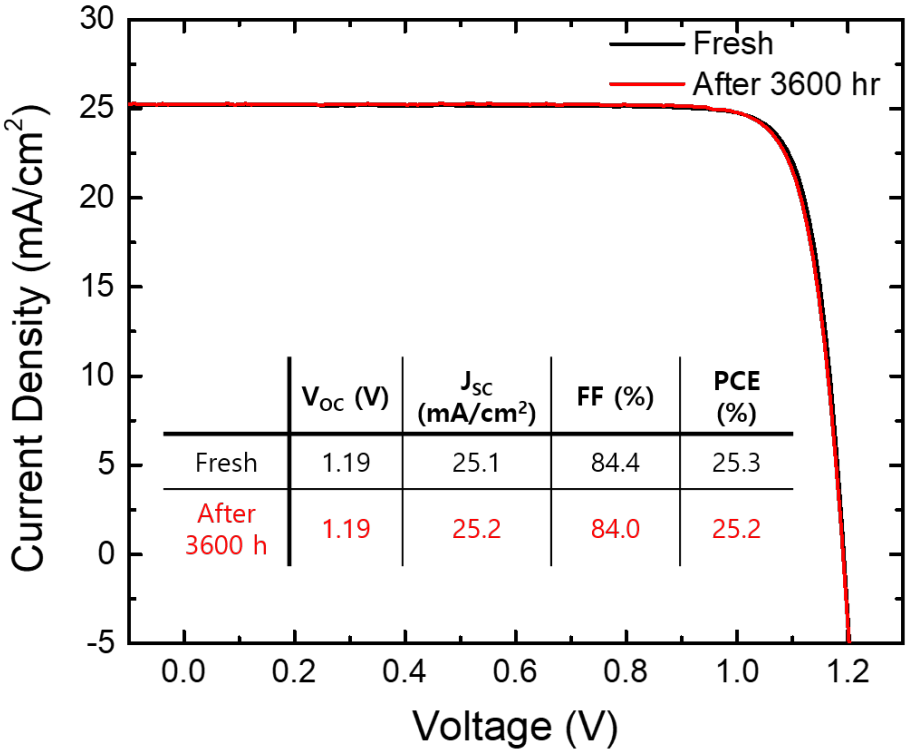

Supplementary Figure 22.

In-house measurements of reverse *J-V* sweep and device data of the certified PSC, measured 3600 hr after certification at Newport. The device was stored in a RH 30% environment with an epoxy/glass encapsulation.

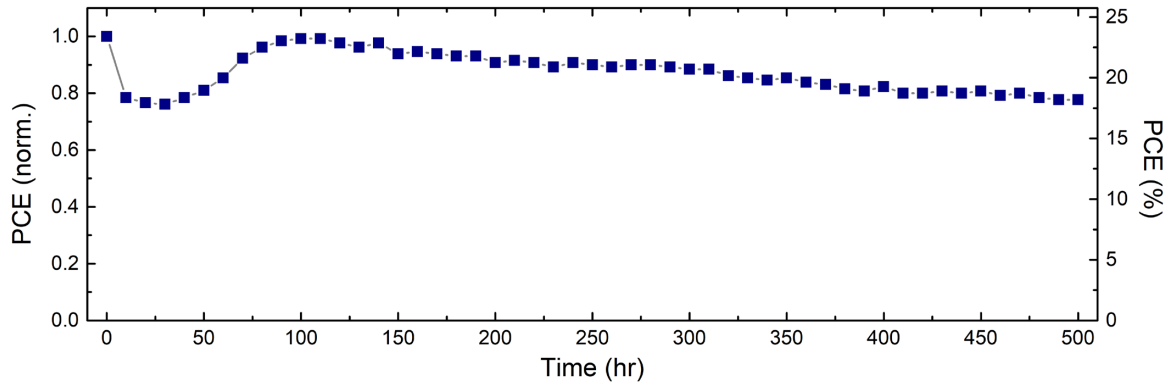

Supplementary Figure 23.

Long-term photostability test under AM 1.5G solar irradiation.

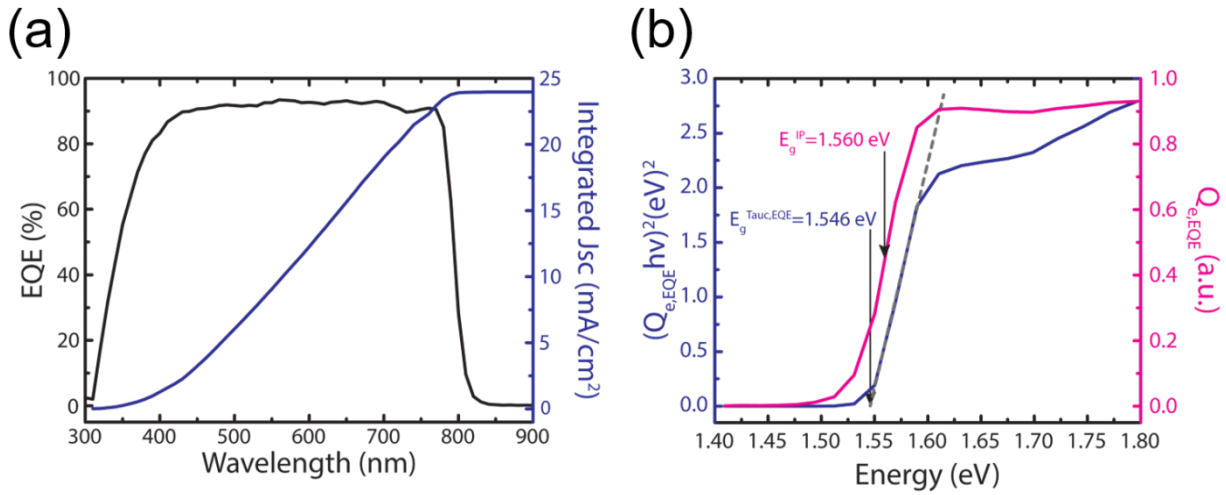

Supplementary Figure 24.

(a) EQE, and integrated J_{SC} of the champion device shown in Figure 4b. (b) Bandgap analysis of the champion device.

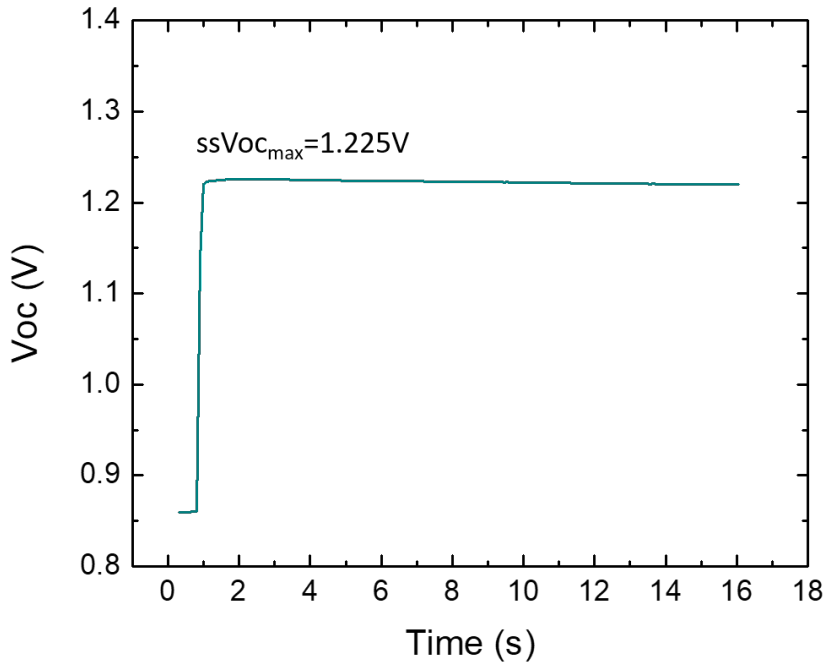

Supplementary Figure 25.

Plot of steady-state V_{OC} (ssV_{OC}) versus time. The ssV_{OC} was measured without a mask and the entire active area was illuminated.

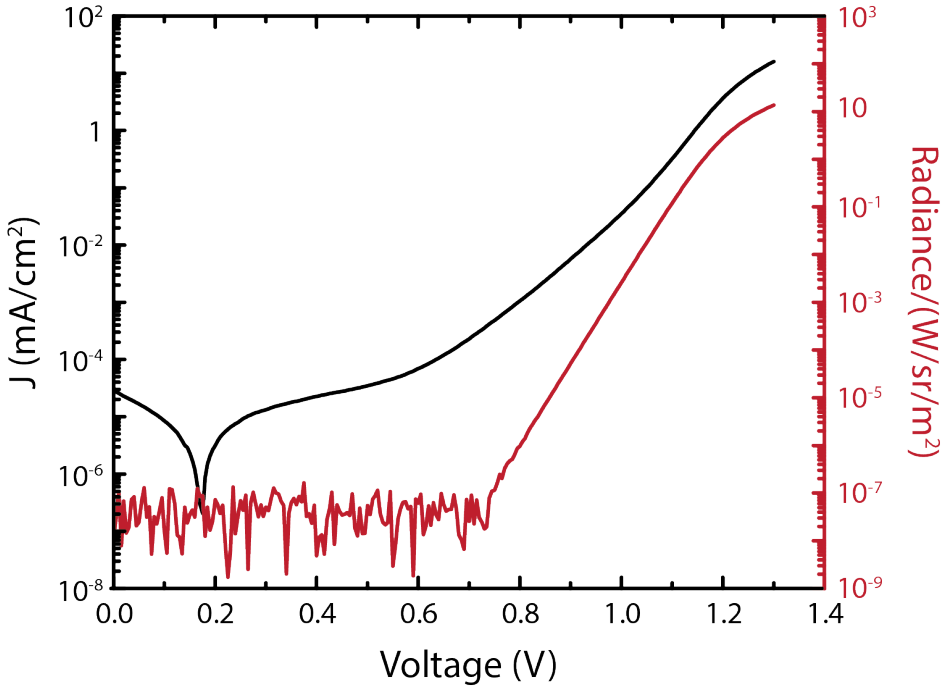

Supplementary Figure 26.

Plot of current density (J) and radiance versus voltage.

References

1. Diekmann, J. *et al.* Pathways towards 30% efficient perovskite solar cells. Preprint at https://arxiv.org/abs/1910.07422 (2019).
2. Le Corre, V. M. *et al.* Charge Transport Layers Limiting the Efficiency of Perovskite Solar Cells: How To Optimize Conductivity, Doping, and Thickness. *ACS Appl. Energy Mater.* **2**, 6280–6287 (2019).
3. Bu, T. *et al.* Universal passivation strategy to slot-die printed SnO_2 for hysteresis-free efficient flexible perovskite solar module. *Nat. Commun.* **9**, 4609 (2018).
4. Abdi-Jalebi, M. *et al.* Maximizing and stabilizing luminescence from halide perovskites with potassium passivation. *Nature* **555**, 497–501 (2018).
5. Son, D.-Y. *et al.* Universal Approach toward Hysteresis-Free Perovskite Solar Cell via Defect Engineering. *J. Am. Chem. Soc.* **140**, 1358–1364 (2018).
6. Park, B. *et al.* Understanding how excess lead iodide precursor improves halide perovskite solar cell performance. *Nat. Commun.* **9**, 3301 (2018).
7. Jacobsson, T. J. *et al.* Unreacted PbI_2 as a Double-Edged Sword for Enhancing the Performance of Perovskite Solar Cells. *J. Am. Chem. Soc.* **138**, 10331–10343 (2016).
8. Xie, F. *et al.* Vertical recrystallization for highly efficient and stable formamidinium-based inverted-structure perovskite solar cells. *Energy Environ. Sci.* **10**, 1942–1949 (2017).
9. Kim, M. *et al.* Methylammonium Chloride Induces Intermediate Phase Stabilization for Efficient Perovskite Solar Cells. *Joule* **3**, 2179–2192 (2019).
10. Khenkin, M. V. *et al.* Consensus statement for stability assessment and reporting for perovskite photovoltaics based on ISOS procedures. *Nat. Energy* **5**, 35–49 (2020).
11. Liu, L. Z., Li, T. H., Wu, X. L., Shen, J. C. & Chu, P. K. Identification of oxygen vacancy types from Raman spectra of SnO_2 nanocrystals. *J. Raman Spectrosc.* **43**, 1423–1426 (2012).